Canard Explosion and Coherent Biresonance in the Rate Oscillation of CO Oxidation on Platinum Surface

Gang Zhao, Zhonghuai Hou,* and Houwen Xin

Department of Chemical Physics, University of Science and Technology of China, Hefei, Anhui, 230026, People's Republic of China

Received: February 22, 2005; In Final Form: July 13, 2005

The relationship between canard explosion and coherent biresonance is analyzed by numerically investigating a temporal dynamical model of CO oxidation on Pt surface. Canard explosion, manifesting itself by a dramatic change in the amplitude and period of a periodic orbit within a very narrow interval of a control parameter, is the result of multiple time scales in a dynamical system and is common in excitable systems. Coherent biresonance, namely, two peaks on the signal-to-noise ratio (SNR) curve when varying noise intensity, is a novel phenomenon of coherent resonance which is well-known in excitable systems. When the control parameter is varied from a stable fixed point, crossing the supercritical Hopf bifurcation, one of the peaks that corresponds to relatively larger noise intensity, keeps a constant height and position, while the other becomes higher and moves to lower noise level. When we consider the case in which two control parameters are perturbed by independent noise simultaneously, an interesting picture of one valley between two ridges appears on the 3D surface of SNR.

Introduction

Canard explosion, a complex temporal behavior resulting from multiple time scales in a dynamical system, has been observed in physical,[1,2] chemical,[3−8] and biological[9,10] systems. It is associated with a dramatic change of period and amplitude of a periodic orbit within a very narrow interval of a control parameter and has been well-understood in the context of singular perturbation theory.[11−13] As a certain control parameter increases beyond the Hopf bifurcation point, the amplitude and period of the limit cycle first increases slowly, with these small amplitude oscillations being termed as canard trajectory; then in an exponentially small neighborhood of some critical point, the so-called canard point, the limit cycle explodes, becoming a relaxation oscillator with much larger amplitude and period. A schematic plot of canard explosion is shown in Figure 1. Canard explosion has the same mathematical source as excitability, and it is reasonable to try to find one when another is present.[3] Excitability is related to a system that is before the Hopf bifurcation point and has only a stable steady state. If perturbed slightly, the system would return to the steady state immediately. Larger perturbations that are beyond a well-defined threshold, however, would cause the system to return to the steady state after a long excursion. This excitable property is important for wave propagation in spatially extended systems. Similar to the excitability of the steady state that is before the Hopf bifurcation point, the oscillatory mode of the small limit cycle (canard trajectory), which is after the Hopf bifurcation point and separated from the large relaxation limit cycle by the canard point, also displays excitable properties. The threshold in this case is the distance to the canard point. Perturbations that are large enough to drive the system through the canard point would induce a large-amplitude relaxation cycle. The connection of excitability and canard explosion suggests that waves can also exist in the vicinity of the canard point and behaves more complexly for it contains the phase information of the canard trajectory other than a stable state.[14] Moreover, the abrupt increase of amplitude and period in canard explosion induces a kind of parametric sensitivity, which is due to the interplay of stable and unstable boundary layers, hence involves strong nonlinearity that would even lead to chaos in some cases.[6,8,15] Although canard explosion is expected to be difficult to observe experimentally, their presence may be inferred from the transition from harmonic oscillations to relaxation oscillations or the so-called mixed mode oscillations,[7] which have been observed in CO oxidation on Pt(110).[16]

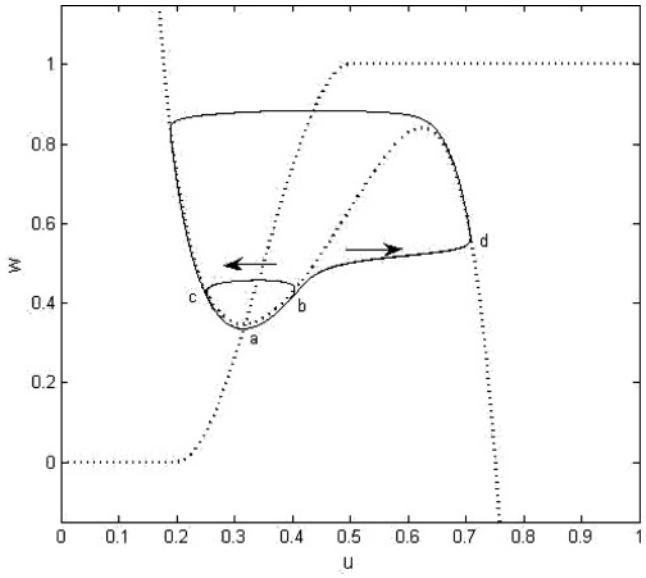

Figure 1. A schematic plot of trajectories before and after canard explosion. Dot lines are nullclines. abca is a canard trajectory; abdca is a relaxation loop after canard explosion.

On the other hand, for real systems, strictly speaking, noise is never zero. In the last two decades, the constructive roles of

* Corresponding author. E-mail address: hzhlj@ustc.edu.cn.

10.1021/jp050907p CCC: $30.25
Published on Web 09/01/2005

noise and disorder in nonlinear systems have been extensively studied. It is now an active subject to researchers from various fields of science that how noise would change the dynamics and functional features of the deterministic system.[17] Specifically, it has been demonstrated that there exists a "resonant" noise intensity at which the response of a system to a periodic force is maximally ordered, which is well-know as stochastic resonance (SR), or the order of the response of an excitable system shows a maximum in the absence of periodic forcing, which is called coherent resonance (CR).[18−25] Recently, attention has been paid to internal noise that is inherent in chemical reactions because of the stochastic nature of the elementary processes including reaction and diffusion.[26] If systems of finite volume are concerned, internal noise must be included in the dynamics, and similar results to external noise are obtained.[27−35]

Since the first observation of rate oscillation in catalytic CO oxidation 35 years ago, dissipative structures in heterogeneous catalytic reactions have been an attractive field in surface science, not only for its richness and complexity, but also from a practical point of view.[36] A variety of "dissipative structures"[37] have been observed in heterogeneous catalytic reactions, including multistability, oscillation, chaos, wave, turbulence, and pattern formation.[38] To understand these interesting phenomena which are also of practical importance, on the basis of mechanisms that had been verified by experiments, various dynamical models, successfully reproducing those experimentally observed phenomena, have been put forward. These models have been employed in testing hypotheses for reaction mechanisms and motivating and selecting further experimental investigations to clarify vague mechanistic issues.[39] Then, progress has been made in controlling spatiotemporal pattern formation in heterogeneous catalytic reactions by prepatterned surface[40] and in improving the reaction performance such as selectivity and reaction rates by, for example, periodic perturbations of reactant concentrations, temperature, or flow reversal.[41]

In the present paper, we investigate the response of the reaction rate of CO oxidation on platinum to external noise. We have done a simple work on the model before.[42] The dynamics of this system, which is described by three ordinary differential equations, undergoes canard explosion shortly after a supercritical Hopf bifurcation.[7] Noise may drive the system from the global steady state that is before the Hopf bifurcation point into the region of canard trajectory or the region of large-amplitude relaxation oscillation, the two regions being separated by the canard point. The consecutive changes of the nature of steady solutions in a narrow interval cause two maxima on the effective signal-to-noise ration (SNR) curve, when varying noise intensity. It may be called coherent biresonance, more concise than the term of stochastic biresonance without external signal.[42] Moreover, the two peaks show different behaviors when the control parameter is varied. We think that canard explosion is the very cause of two peaks, and their different behaviors can be understood by considering the different properties of canard trajectory and the relaxation oscillation. The result of this paper also demonstrates a noise-select effect in the vicinity of the canard point: the amplitude and period of reaction rate oscillation are selected via noise intensity.

Model

The model we used in the present paper was developed to describe the temporal dynamics of CO oxidation on the Pt (110) surface. This Krischer−Eiswirth−Etrl model[16] is a realistic model for surface coverage and describes the experimental phenomenon at ultrahigh-vacuum (UHV) conditions very well. The mechanism of CO oxidation on platinum proceeds via the Langmuir−Hinshelwood scheme, in which both CO and O_2 have to adsorb onto the catalytic Pt surface before reacting with each other

$$CO + * \rightleftarrows CO_{ad}$$

$$O_2 + 2* \rightarrow 2O_{ad}$$

$$O_{ad} + CO_{ad} \rightarrow CO_2 + 2*$$

Here, the asterisk (*) denotes a free adsorption site, and the subscript ad denotes an adsorbed species. There is an adsorbate-driven surface structural transition based on the CO coverage, which is essential for rate oscillations.

$$1 \times 2 \overset{CO_{ad}}{\rightleftharpoons} 1 \times 1$$

The above mechanism is modeled by the following three equations:[16]

$$\begin{aligned} \frac{du}{dt} &= p_{CO} k_c s_c \left(1 - \frac{u}{u_s}\right)^3 - k_d u - k_r u v \\ \frac{dv}{dt} &= p_{O_2} k_o s_o \left(1 - \frac{u}{u_s} - \frac{v}{v_s}\right)^2 - k_r u v \\ \frac{dw}{dt} &= k_p [h(u) - w] \end{aligned} \tag{1}$$

Here, p_{CO} and p_{O_2} are partial pressure of CO and O_2, u is the surface coverage of CO, v is the surface coverage of O, and w is the fraction of the surface area exhibiting the 1×1 structure. The variables u, v, and w must be in the interval [0, 1]. The sticking coefficient of oxygen depends on the surface structure and is given by $s_O = w s_{O1} + (1 - w) s_{O2}$. The function $h(u)$ is experimentally established to account for the structural phase transition of the Pt (110) surface.

$$h(u) \equiv \begin{cases} 0 & u \le 0.2 \\ \sum_{i=0}^{3} r_i u^i & 0.2 \le u \le 0.5 \\ 1 & u > 0.5 \end{cases}$$

$r_3 = -1/0.0135$, $r_2 = -1.05\ r_3$, $r_1 = 0.3\ r_3$, $r_0 = -0.026\ r_3$. The reaction rates k_r, k_d, and k_p are Arrhenius-formulated: $k_i = k_{i0} \exp[-E_i/RT]$, $i = r, d, p$. Other constants used in this model are in ref 7.

The bifurcation diagram of the deterministic model with T fixed at 540 K is presented in Figure 2a. It is the same as Figure 8 in ref 16 and is reproduced with the help of Matcont,[43] a continuation software in Matlab. See the figure captions for details. The stable states in the left area of the curves correspond to oxygen-covered surface, and the right area corresponds to the CO-covered surface. Our numerical studies are mainly carried out on the solid arrow (AB), which is slightly above the upper Hopf bifurcation branch, and the dashed arrow, which is vertical with $p_{CO} = 45.5 \times 10^{-6}$ mbar.

The bifurcation details on the dashed arrow (Figure 2a) are plotted in Figure 2b; note that the abscissa axis is not in scale. From Figure 2b, one can easily divide the parameter scope into four regions: (1) one stable node; (2) small-amplitude oscillation (canard trajectory) created by a supercritical Hopf bifurcation (HB) at $p_{O_2} \approx 151.058 \times 10^{-6}$ mbar coexisting with one unstable focus; (3) large-amplitude relaxation oscillation, started by canard explosion at $p_{O_2} \approx 150.7582 \times 10^{-6}$ mbar, ended in

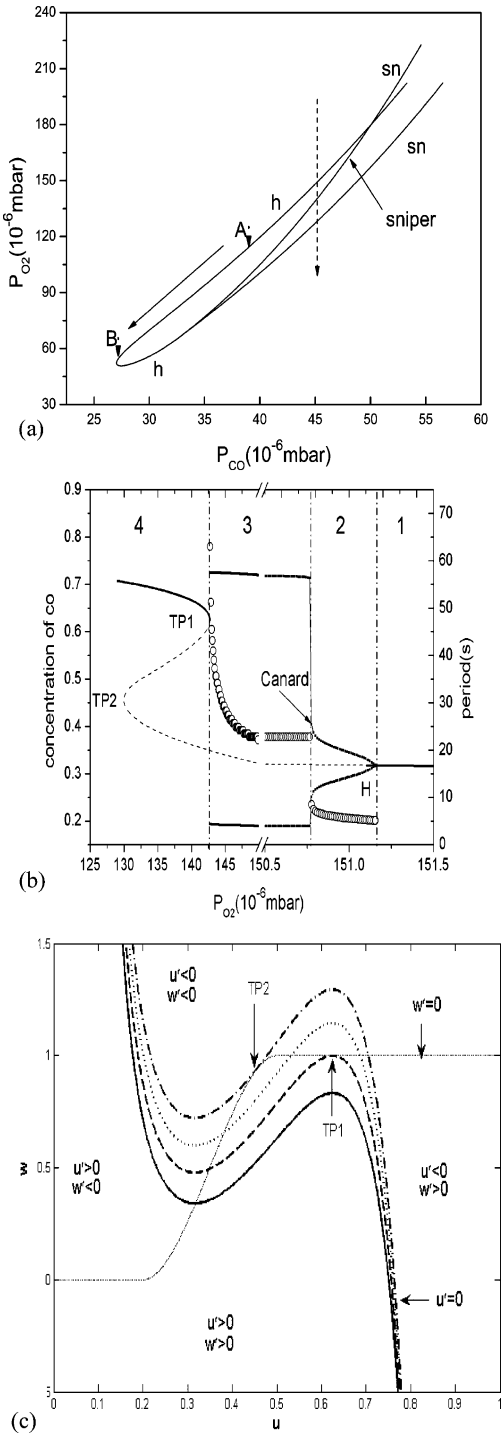

Figure 2. (a) Bifurcation diagram of the model (1) with T fixed at 540 K. The labels h, sn, and sniper are Hopf bifurcation, saddle-node bifurcation of fixed points, and saddle-node of infinite period bifurcation, respectively. The solid arrow (AB) and the dashed arrow indicate where numerical simulations have been carried out. (b) The bifurcation details on the dashed arrow in (a). Note that the abscissa axis is broken to show details of canard explosion. H denotes Hopf bifurcation. Circles are periods (right axis) of the corresponding oscillations. Squares are maximum and minimum in the oscillation of the concentration of CO (left axis). Lines are steady points of the model: solid, stable; dash, unstable. The three vertical dash−dot lines are to help the eyes in dividing the parameter scope into four regions. (c) Nullclines of the reduced model. Circles are nullcline of $\dot{w} = 0$. Those that are S-shaped are nullclines of $\dot{u} = 0$ with different control parameters. From bottom to top, respectively, Hopf bifurcation (solid); sniper (dash); a complementary line (dot) to show the coexisting three steady state in region 4, and saddle-node bifurcation (dash dot). The scale of w is out of physical bound to give a full exhibition of the nullclines.

saddle-node infinite period (sniper) at turning point 1 (TP1) with $p_{O_2} \approx 142.753 \times 10^{-6}$ mbar, coexisting with the unstable focus; (4) a saddle-node pair of fixed points, coexisting with one unstable focus. The saddle and the unstable focus annihilate each other at turning point 2 (TP2) with $p_{O_2} \approx 130.006 \times 10^{-6}$ mbar.

We give in Figure 2C a complementary interpretation of what happened on the dashed arrow by drawing the nullclines of $\dot{u} = 0$ and $\dot{w} = 0$ in the $w \sim u$ plane. To draw the nullclines on the $w \sim u$ plane, one should first reduce the dimension to 2, which is originally 3. The validity and the details of the reduction of dimension of this model had been discussed in ref 7. We just plot the nullclines of the reduced model in Figure 2c. From the different intersecting situations of the nullclines, one can easily understand the bifurcation details of the dynamical systems. The nullcline (circle) is $\dot{w} = 0$; it does not change with the value of P_{CO} or P_{O_2} (because of the special form of $h(u)$, see eq 1). The other S-shaped curves are $p_{O_2} = 151.058 \times 10^{-6}$, 142.753×10^{-6}, 136.020×10^{-6}, 130.006×10^{-6} from bottom to top, respectively. Note that the S-shaped nullclines are common in excitability and canard explosion.[4,20] Turning point 1 and turning point 2 are created when the two nullclines are tangent with different branches.

We take noise into account by replacing p_{O2} with $[1 + D*\zeta(t)]*p_{O_2}$ in eq 1. Here, D is noise intensity, and $\zeta(t)$ is a Gaussian white noise with zero mean $\langle \zeta(t) \rangle = 0$ and unit variance $\langle \zeta(t)\zeta(t') \rangle = \delta(t - t')$. We numerically integrate eq 1 using the explicit Euler forward integrating method with a time step $dt = 0.002$ s. We then estimate the power spectral density (PSD) of the time series of u, the coverage of CO. From the PSD data, we can obtain the effective SNR, which is an appropriate measure of order in the study of stochastic oscillation. It is defined as the relative height of the peak in the PSD normalized by its relative width; we refer readers to our previous papers for a graphical explanation and more information of effective SNR.[34,35]

Results and Discussion

To begin, we fix $(P_{CO}, P_{O_2}) = (45.5, 151.5) \times 10^{-6}$ mbar; the system is in region 1 near the Hopf bifurcation point. The corresponding curve of $D \sim$SNR (circle) and the characteristic periods of the reaction rate oscillation (star) are presented in Figure 3a. Two maxima of SNR are clear. We then scan along the dashed arrow from $P_{O_2} = 151.5 \times 10^{-6}$ mbar to $P_{O_2} = 150.8 \times 10^{-6}$ mbar, which covers region 1 and region 2. The 3D surface of $D \sim P_{O_2} \sim$SNR is presented in Figure 3b. One can see distinctly the different behaviors of the two peaks when P_{O_2} is varied. As the system shifts from region 1 to region 2, the peak at low noise intensity becomes higher and moves to lower noise level until it disappears at the starting point of region 2, while the other keeps a constant height and position even in region 2. The presence of a peak in region 2 is especially worth mentioning, because it is contrary to the usual conception that noise would destroy order in oscillating regions.

The results in Figure 3 can be explained by considering two factors. First, sustained noise would drive the system from region 1 into region 2 or region 3, since the width of region 2 is very narrow. While arbitrarily small perturbations can cause the dynamics to small-amplitude oscillations that correspond to a so-called stochastic limit cycle[20] in phase space, only the perturbations large enough to drive the system through the critical canard point would cause the dynamics to display large-relaxation oscillations, in which even a relatively larger noise would not influence the deterministic motion very much during

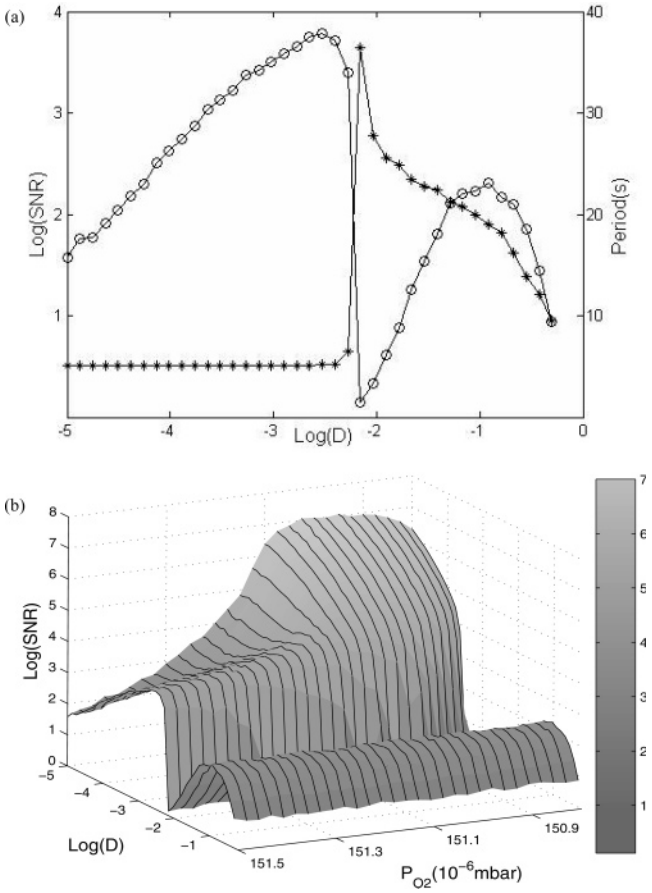

Figure 3. (a) Coherent biresonance and the characteristic periods of reaction rate oscillation. Circles are SNR (left axis); stars are characteristic periods (right axis) of reaction rate oscillation. (b) 3D surface of. $D\sim P_{O_2}\sim$SNR. The control parameter P_{O_2} covers region 1 and region 2. The peak which locates at a relatively lower noise level shifts its position, while the other that has a relatively larger resonant noise level keeps a constant position and height.

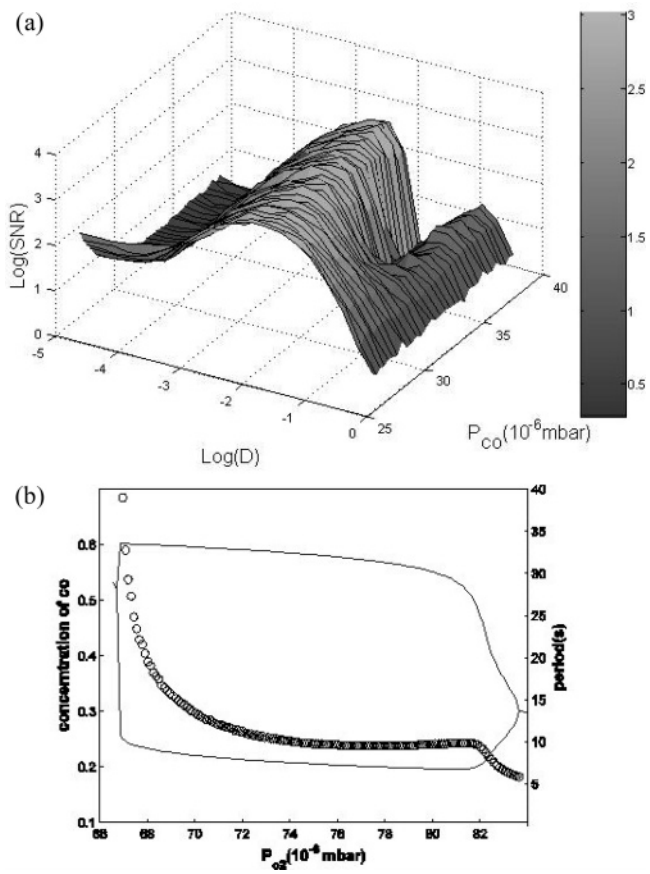

Figure 4. (a) 3D surface of $D\sim P_{O_2}\sim$SNR. When scanning along the solid arrow AB (Figure 2a), the two-peak structure transforms into a one-peak structure. The transition point is numerically found to be at $P_{CO} \approx 32.885 \times 10^{-6}$ mbar. (b) Bifurcation diagram at the transition point. Circles are periods (right axis). Lines are maximum and minimum in the oscillation of the concentration of CO (left axis). Compare with Figure 2b. The increase of period and amplitude of oscillation is now much milder.

its long refractory part.[20] Both types of noise-induced oscillation undergo coherent resonance,[20,22] so it is natural that two peaks appear on the effective SNR curve when noise intensity is varied. Second, for the different behaviors of the two peaks with the variation of P_{O_2} in Figure 3b, we attribute them to the different properties of the canard trajectory and the large relaxation loop as is shown in Figure 2b: with the decrease of P_{O_2}, the amplitude and period of the canard trajectory increases slowly, so the corresponding maximal SNR value increases, while the amplitude and period of the large relaxation loop keeps nearly constant in the vicinity of the canard point (please note the break in the abscissa), so the corresponding maximal SNR value keeps constant. Note that sniper also involves excitable properties;[44] therefore, the SNR curve would show two peaks: one peak, monotonically decreasing behavior, and one peak in regions 1, 2, 3, and 4, respectively (results in region 3 and 4 are not shown).

To get a global knowledge of the noise dynamics of the model, we scan along segment AB (Figure 2, solid arrow). For each run, the system is set slightly above the upper Hopf bifurcation branch by $(P_{CO}, P_{O_2}) = (P^0_{CO}, P^0_{O_2} + 0.1) \times 10^{-6}$ mbar, where $(P^0_{CO}, P^0_{O_2}) \times 10^{-6}$mbar is on the upper Hopf bifurcation branch. A and B are located at $(P^0_{CO}, P^0_{O_2}) = (38.923, 113.906) \times 10^{-6}$ mbar and $(27.043, 52.365) \times 10^{-6}$ mbar, respectively. The 3D surface of $D\sim P_{CO}\sim$SNR is presented in Figure 4a. A transition of structure from two-peak to one-peak is numerically found to be at $P_{CO} \approx 32.885 \times 10^{-6}$ mbar. We find that this is because the explosion of the canard trajectory (increase of the period and amplitude) become milder and milder along the segment AB. The bifurcation diagram at the transition point shown in Figure 4b helps to explain phenomenologically the situation.

To further demonstrate the interesting noisy dynamics related to the deterministic bifurcation features, we fix $(P_{CO}, P_{O_2}) = (45.5, 151.5) \times 10^{-6}$ mbar such that the system is in region 1 and perturb both P_{CO} and P_{O_2} simultaneously by independent Gaussian white noise. The 3D surface of $D_{CO}\sim D_{O_2}\sim$SNR is presented in Figure 5. To show the structure clearly, we have adopted the logarithmic scale for both noise intensities, so there appears in Figure 5 a rectangular structure which is actually an elliptic structure if linear scale is adopted for both noise intensities. The result is rather interesting. First, whether P_{CO} or P_{O_2} is perturbed alone, coherent biresonance would occur in either case. Second, when both P_{CO} and P_{O_2} are perturbed simultaneously, coherent biresonance also occurs along the radial direction. This result confirms the relationship between canard explosion and coherent biresonance as discussed above.

In this paper, we have numerically investigated the effects of parameter noise on CO oxidation on platinum surface, using the pioneer Krischer−Eiswirth−Etrl model, with special concern regarding the relationship between canard explosion and coherent biresonance. After giving a detailed description of specific dynamical features of the model, especially the existence of canard explosion in the vicinity of the Hopf bifurcation, we

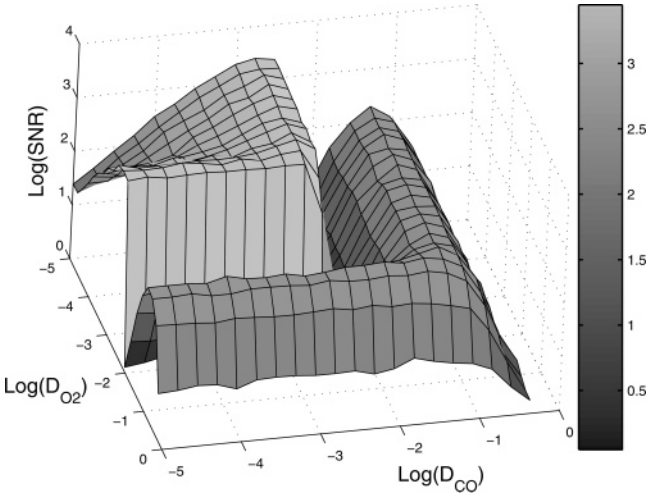

Figure 5. 3D surface of $D_{CO}\sim D_{O_2}\sim$SNR. The rectangular structure is actually an elliptic structure if linear scale is adopted.

carried out simulations to calculate SNR as in the conventional study of coherent resonance. The distinct feature of our results is the bimodal shape of the SNR$\sim D$ curve, indicating the occurrence of coherent biresonance. The relationship between canard explosion and coherent biresonance is established through a thorough numerical study on the $P_{CO}\sim P_{O_2}$ plane. Moreover, we attribute the different behaviors of the two peaks on the $D\sim$SNR$\sim P_{O_2}$ surface to the different oscillation properties of the canard trajectory and the relaxation loop.

Although the present work mainly contributes a model study of CO catalytic oxidation, one may also address a few points of its relevance to the physical basis. First, regarding the ever-growing attention being paid to the constructive roles of noise in nonlinear systems, the results in this paper demonstrated a novel phenomenon, coherent biresonance, by illustrating its very connection to canard explosion. The physical relevance of coherent biresonance shown here, to our opinion, is a kind of noise-selecting effect, i.e., different noise level prefers to sustaining oscillations of different amplitude, frequency, type, and thus different physical functions. Second, the present work may also help narrow the gap between experiments and theoretical study of surface catalytic reactions, bearing in mind that parameter noises are inevitable in real systems. Because of the existence of noise-induced oscillation and coherent biresonance, a stochastic model is expected to show rather different dynamic behavior from the deterministic model, deserving the consideration of noise an important aspect in theoretical modeling and making the control of noise in experiments a more crucial task. Specifically, in the cases when the explosion to large relaxation oscillations is required to avoid (for instance, a simple numerical calculation revealed that the production rate of CO_2 in region 3 is much smaller than those in region 2 and 1), the present study helps to clarify the upper boundary of the noise intensity. Finally, canard explosion has been found in many chemical and physical systems, and of more significance, in biological systems . We note that an interesting feature of the canard phenomenon is that it combines both high sensitivity and high robustness to noise. The high sensitivity is relevant with the supercritical Hopf bifurcation, where an ultrasmall noise can induce sustained oscillation with rather high SNR. While the robustness is associated with the excitability to relaxation oscillation, of which the period and amplitude is robust to the change of noise intensity. Noting that highly sensitivity and robustness are both of great biological interest, one would expect that our present work, connecting canard phenomenon and coherent biresonance, may also find interesting applications in real living systems.

Acknowledgment. This work is supported by the National Science Foundation of China (20203017, 20433050), and the Foundation for the Author of National Excellent Doctorial Dissertation of PR China (FANEDD).

References and Notes

(1) Benoit, E.; Callot, J. L.; Diener, F.; Diener, M. *Collect. Math.* **1981**, *32*, 37.
(2) Diener, M. *Math. Intell.* **1984**, *6*, 38.
(3) Bar-Eli, K.; Brøns, M. *J. Phys. Chem.* **1990**, *94*, 7170.
(4) Brøns, M.; Bar-Eli, K. *J. Phys. Chem.* **1991**, *95*, 8706.
(5) Milik, A.; Szmolyan, P.; LÖffelmann, H.; GrÖller, E. *Int. J. Bifurcation Chaos Appl. Sci. Eng.* **1998**, *8*, 505.
(6) Brøns, M.; Sturis, J. *Phys. Rev. E* **2001**, *64*, 026209.
(7) Moehlis, J. *J. Nonlinear Sci.* **2002**, *12*, 319.
(8) Chumakov, G. A.; Chumakova, N. A. *Chem. Eng. J.* **2003**, *91*, 151.
(9) Kakiuchi, N.; Tchizawa, K. *J. Diff. Eq.* **1997**, *141*, 327.
(10) Guckenheimer, J.; Hoffman, K.; Weckesser, W. *Int. J. Bifurcation Chaos Appl. Sci. Eng.* **2000**, *10*, 2669.
(11) Grasman, J. *Asymptotic Methods for Relaxation Oscillations and Applications*; Springer-Verlag: New York, 1987.
(12) Mishchenko, E. F.; Kolesov, Yu. S.; Kolesov, A. Yu.; Rozov, N. Kh. *Asymptotic methods in singularly perturbed systems*; Consultants Bureau: New York and London, 1994.
(13) Krupa, M.; Szmolyan, P. *J. Diff. Eq.* **2001**, *174*, 312.
(14) Buchholtz, F.; Dolnik, M.; Epstein, I. R. *J. Phys. Chem.* **1995**, *99*, 15093.
(15) Deng, B. *Chaos* **2004**, *14*, 1083.
(16) Krischer, K.; Eiswirth, M.; Ertl, G. *J. Chem. Phys.* **1992**, *96*, 9161.
(17) *Proceedings of the 16th International Conference on Noise in Physical Systems and 1/f Fluctuations*; Bosman, G., Ed.; World Scientific: Singapore, 2001.
(18) Gammaitoni, L.; Hanggi, P.; Jung, P.; Marchesoni, F. *Rev. Mod. Phys.* **1998**, *70*, 223.
(19) Hanggi, P. *ChemPhysChem.* **2002**, *3*, 285.
(20) Lindner, B.; Garcia-Ojalvo, J.; Neiman, A.; Schimansky-Geier, L. *Phys. Rep.* **2004**, *392*, 321.
(21) Kiss, I. Z.; Hudson, J. L.; Santos, G. J. E.; Parmananda, P. *Phys. Rev. E* **2003**, *67*, 035201.
(22) Hu, G.; Ditzinger, T.; Ning, C. Z.; Haken, H. *Phys. Rev. Lett.* **1993**, *71*, 807.
(23) Lin, I.; Liu, J. M. *Phys. Rev. Lett.* **1995**, *74*, 3161.
(24) Santos, G. J. E.; Rivera, M.; Eiswirth, M.; Parmananda, P. *Phys. Rev. E* **2004**, *70*, 021103.
(25) Miyakawa, K.; Isikawa, H. *Phys. Rev. E* **2002**, *66*, 046204.
(26) van Kapman, N. G. *Stochastic Processes In Physics and Chemistry*; North-Holland: Amsterdam, 1987.
(27) Hildebrand, M.; Mikhailow, A. S.; Erlt, G. *Phys. Rev. E* **1998**, *58*, 5483.
(28) Shuai, J. W.; Jung, P. *Phys. Rev. Lett.* **2002**, *88*, 068102.
(29) Schmid, G.; Goychuk, I.; Haggi, P. arXiv.org; http://arxiv.org/abs/physics/0106036.
(30) Suchorski, Y.; Beben, J.; James, E. W.; Evans, J. W.; Imbihl, R. *Phys. Rev. Lett.* **1999**, *82*, 1907.
(31) Hildebrand, M.; Mikhailov, A. S.; Ertl, G. *Phys. Rev. Lett.* **1998**, *81*, 2602.
(32) Zhang, J.; Hou, Z.; Xin, H. *ChemPhysChem.* **2004**, *5*, 1041.
(33) Gong, Y.; Hou, Z.; Xin, H. *J. Phys. Chem B* **2004**, *108*, 17796.
(34) Hou, Z.; Xin, H. *J. Chem. Phys.* **2003**, *119*, 11508.
(35) Hou, Z.; Xin, H. *ChemPhysChem.* **2004**, *3*, 407.
(36) Thomas, J. M.; Thomas, W. J. *Principles and Practice of Heterogeneous Catalysis*; VCH: Weinheim, 1997.
(37) Nicolis, G.; Prigogine, I. *Self-Organization in Nonequilibrium Systems*; Wiley: New York, 1977.
(38) Imbihl, R.; Ertl, G. *Chem. Rev.* **1995**, *95*, 697.
(39) Lebiedz, D.; Brandt-Pullmann, U. *Phys. Rev. E* **2004**, *70*, 051609.
(40) Graham, M. D.; Kevrekidis, I. G.; Asakura, K. *Science* **1994**, *264*, 80.
(41) Zhdanov, V. P. *Surf. Sci. Rep.* **2004**, *55*, 1 and references therein.
(42) Hou, Z.; Yang, L.; Xin, H. *J. Chem. Phys.* **1999**, *111*, 1592.
(43) http://allserv.rug.ac.be/~ajdhooge/research.html.
(44) Dilão, R.; Volford, A. *Dis. & Con. Dyn. Sys. B* **2004**, *4*, 419.